SOILS AND FOUNDATIONS Vol. 38, No. 4,195-203, Dec. 1998
Japanese Geotechnical Society

NON-SYMMETRICAL LIMIT LOADS ON STRIP FOOTINGS

RADOSLAW L. MICHALOWSKI[i] and LIANGZHI YOU[i]

ABSTRACT

Limit loads on footings (bearing capacity) can be conveniently analyzed using the kinematic approach of limit analysis. Nonsymmetrical loads on strip footings include the horizontal component of the load and the moment. They can be also represented as load inclination and eccentricity. For the analysis to be sensitive to nonsymmetrical loads, the collapse mechanisms also need to be nonsymmetrical, i.e., they need to allow for footing rotation and horizontal component of displacement. Based on such mechanisms, inclination coefficients for surface strip footings are derived. These coefficients fit the numerical limit analysis results better than the coefficients suggested earlier in the literature. It is also shown that for cohesive-frictional soils the method often used to account for the load eccentricity (where the footing width is reduced by twice-the-eccentricity) yields a bearing capacity lower than that obtained from the kinematic limit analysis. However, this method overestimates the bearing capacity for purely frictional soils, particularly when the surcharge load is small.

Key words: bearing capacity, failure, foundation, limit state design, load eccentricity, load inclination, plasticity (**IGC**: E3)

INTRODUCTION

Limit loads on footings are typically calculated from an expression which contains three terms, dependent on the soil cohesion, surcharge load, and the soil weight, respectively. A complete closed-form solution to the problem is known only for strip footings on weightless soils, and loaded with vertical loads (Prandtl, 1920; Reissner, 1924). Nonsymmetrical loads include horizontal forces and moments. Moments are always associated with horizontal loads applied above the footing level. Moments also can be induced by eccentricity of vertical loads. Typically, moments are given in analyses as eccentricity e of the vertical load, independent of their origin, e.g., the wind load or inertial forces due to seismic shaking, can be described in terms of the horizontal load and vertical load eccentricity.

This paper uses the concept of *generalized stresses* and *generalized strains*, as suggested in structural mechanics by Prager (1955), and often employed in limit state analysis of structures. The variety of possible footing responses to different loads (symmetric and nonsymmetric) can be considered. The notion of generalized loads was more recently used in analysis of bearing capacity of surface footings by Gottardi and Butterfield (1993), and Salençon and Pecker (1995).

Limit analysis is used in this paper to explore failure modes of strip footings under nonsymmetrical loads. Failure criteria which relate to these modes are then interpreted as failure surfaces in the space of generalized stresses. The concept of generalized stresses and strains is explained in the next section, followed by the analysis of different failure modes of strip footings. Conclusions are then made as to how the inclined forces and moments (eccentricity of load) can be included in calculations of bearing capacity, and whether the existing methods should be modified.

GENERALIZED DESCRIPTION

Generalized Stresses and Strains

Prager (1955) indicated that plastic analysis of structures could be simplified if one introduced forces and bending moments in structural members (such as beams, columns, and frames) as *generalized stresses* (Q_i), and the corresponding displacement and rotation rates as *generalized strain rates* ($\dot{q}_i$). He then suggested that the yield condition and the plastic flow rule be expressed for the entire structure in term of those forces and strain rates. Generalized stresses and strain rates are defined such that their rate of work, $\dot{W}$, can be expressed as

$$\dot{W}=Q_1\dot{q}_1+Q_2\dot{q}_2+Q_3\dot{q}_3+\cdots+Q_n\dot{q}_n. \quad (1)$$

The yield condition for a structure is then expressed in terms of Q_i as

[i] Department of Civil Engineering, The Johns Hopkins University, Baltimore, MD 21218, USA.
Manuscript was received for review on September 8, 1997.
Written discussion on this paper should be submitted before July 1, 1999 to the Japanese Geotechnical Society, Sugayama Bldg. 4F, Kanda Awaji-cho, 2-23, Chiyoda-ku, Tokyo 101-0063, Japan. Upon request the closing date may be extended one month.

$$f(Q_1, Q_2, Q_3, \cdots, Q_n)=0 \tag{2}$$

and the generalized associative flow rule is

$$\dot{q}_i=\dot{\lambda}\frac{\partial f(Q_k)}{\partial Q_i}, \quad \begin{matrix}\dot{\lambda}=0 \text{ if } f<0 \\ \dot{\lambda}\geq 0 \text{ if } f=0\end{matrix} \tag{3}$$

where $\dot{\lambda}$ is a scalar multiplier. For instance, the yield condition of beams can be described with only one constant—the yield moment, with the rate of curvature being the generalized strain rate. The yield criterion of a thin plate, on the other hand, is a function of two bending moments and a twisting moment, and the respective generalized strain rates are two curvature rates and a rate of twist. This concept can be extended to footings as presented in the next subsection.

Bearing Capacity of Footings in Terms of Generalized Stresses and Strains

Generalized stresses can be extended to loads on a structure. For a strip footing these are: vertical force P, horizontal force T, and in-plane moment M (or Q_1, Q_2 and Q_3). The corresponding generalized strain rates are: the vertical displacement rate of the footing (rate of plastic settlement), horizontal velocity, and the rate of the footing rotation, respectively. Consequently, the limit state of a strip footing can be represented as a convex surface in space P, T, M, and it is shown schematically in Fig. 1(a). This is a composite surface (usually not symmetrical) with its different regions corresponding to different failure modes.

The solid line in Fig. 1(b) shows the cross-section of surface $f(P, T, M)=0$ with plane $M=$const. Each of the segments of this line relates to one specific failure mechanism of the footing. For instance, segment OK relates to a rigid rotation mechanism, whereas segment KH is associated with a translational mechanism. Segment OGH relates to a mechanism where the footing and the soil immediately underneath rotate as one rigid body, while the soil in the other parts of the mechanism undergoes continual shearing. The dashed line in Fig. 1(b) represents limit loads for translational and rigid rotation mechanisms which yield larger limit loads (not as good) for footings loaded eccentrically. All of these mechanisms are described in detail in the next Section.

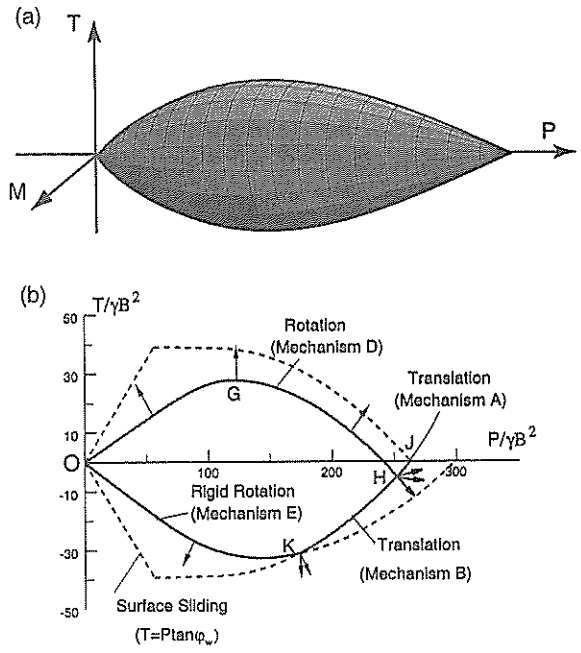

Fig. 1. Failure criterion for strip footings: (a) schematic of a failure surface in the load space; and (b) cross-section of a failure surface for $M=$const.

If a space of generalized strain rates is superimposed on the space P, T, M, the footing displacement and rotation rates can be, according to the normality rule in Eq. (3), represented by vectors perpendicular to the yield surface. The corner points (K and H) signify that there may be more than one displacement mode related to one set of loads. The displacement rate at such points is a linear combination of rates for the mechanisms represented at that point (Koiter, 1953).

Limit analysis will be employed to determine the shape of the yield surface. Specific failure mechanisms corresponding to different regions of the generalized yield surface are analyzed in the next section.

LIMIT ANALYSIS

The Upper-Bound Approach

Limit analysis is a convenient tool for estimating the bearing capacity of footings, and it is used here to determine failure loads on footings subjected to nonsymmetrical loads. The kinematic theorem of limit analysis was used recently for a very similar problem (Michalowski, 1997), and the details of application of this theorem can be found therein. The theorem states that *the rate of work dissipation is not less than the rate of work of external forces for any kinematically admissible collapse mechanism*. This can be written as

$$\int_V \dot{D}(\dot{\varepsilon}_{ij})dV \geq Q_i q_i+\int_V \gamma_i v_i dV+\int_S \bar{q}_i v_i dS \tag{4}$$

where γ_i is the specific weight vector, v_i is the velocity vector in the kinematically admissible mechanism, $\bar{q}_i$ is the surcharge vector, V and S are the mechanism volume and surface, respectively, and $Q_i q_i$ is the work of external loads applied to the footing (summation convention holds; *see* Eq. (1)).

Based on inequality (4) an upper bound to the limit load can be found. The external forces, in the case of a footing, include the surcharge load, soil weight, and the load on the footing P, T and M (or Q_1, Q_2 and Q_3). One of the load components can be unknown, while the other two must be given. By repeating calculations for different combinations of the external loads one can trace the entire failure surface.

Mechanisms of Soil Yielding Under a Strip Footing

Mechanisms of foundation soil failure considered here are presented in Figs. 2–7. These mechanisms are de-

scribed by letters A through E. In order for the limit analysis to be sensitive to nonsymmetrical loads, mechanisms must include nonsymmetrical displacement modes. The mechanisms selected here are the most realistic collapse modes which are expected to yield the least upper bounds to the bearing capacity for a variety of combinations of eccentricity and horizontal loads.

For calculations to be sensitive to an inclined load (or horizontal load component), the mechanism must allow for horizontal displacement of the footing. Otherwise the work of the horizontal load component is zero, and the bearing capacity is independent of the magnitude of T. Similarly, if the solution to the bearing capacity is to be dependent on the moment (or eccentricity), the mechanism in limit analysis must involve the footing rotation.

The multi-block translational mechanism in Fig. 2(a) has a symmetrical geometry, with the rigid blocks separated by the velocity discontinuities. When the number of blocks tends to infinity, this mechanism becomes similar to the one associated with the static solution of Prandtl (1920). Notice that, even if the geometry of the mechanism is symmetrical, the footing displacement may be nonsymmetrical, as presented by the hodograph in Fig. 2(c). This mechanism is not sensitive to footing rotation, and the limit loads calculated based on this mechanism correspond to point J in Fig. 1(b).

A nonsymmetrical (one-sided) mechanism of a similar type is shown in Fig. 3(a), and a particular case of this mechanism is shown in Fig. 4(a). Collapse mechanisms in Figs. 5–7 all involve rotation of the footing. Deformation patterns in Fig. 5 and Fig. 6 are alike, with the latter permitting a separation of the footing from the ground surface. Similar patterns were used by Murff and Miller (1977) and, more recently, by Salençon and Pecker

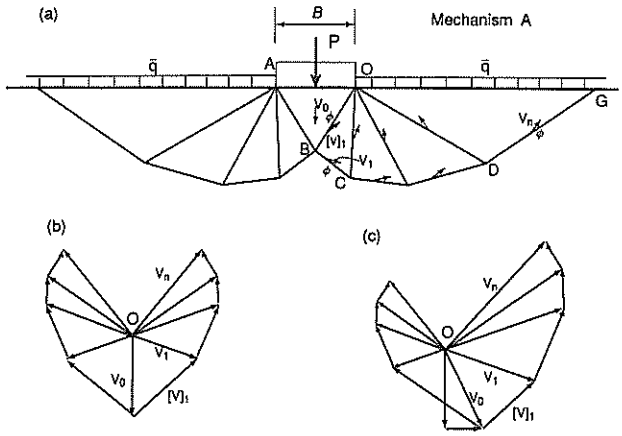

Fig. 2. Translational failure mode (Mechanism A): (a) rigid-block collapse pattern; (b) hodograph for vertical displacement of the footing; and (c) hodograph for nonsymmetrical displacement pattern

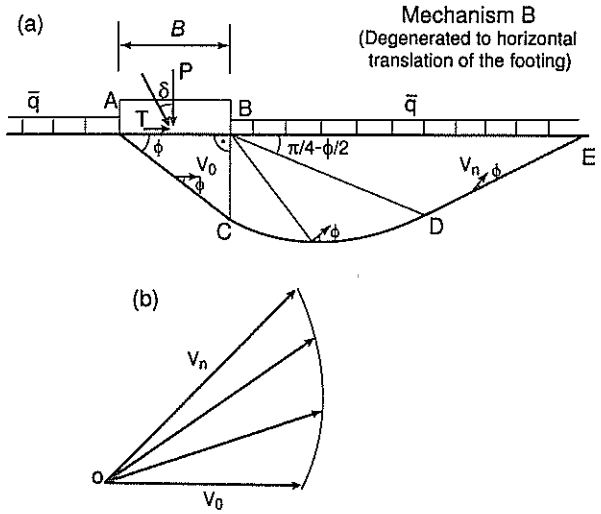

Fig. 4. Mechanism associated with horizontal displacement of the footing (degenerated Mechanism B): (a) failure pattern; and (b) hodograph

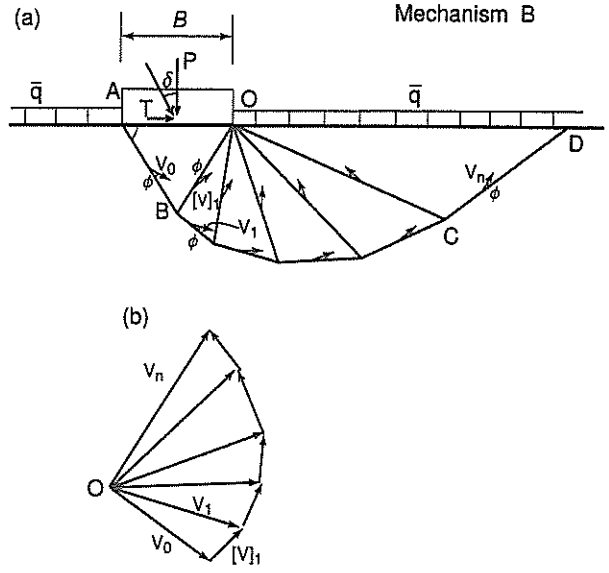

Fig. 3. Nonsymmetric translational mode (Mechanism B): (a) collapse pattern; and (b) hodograph

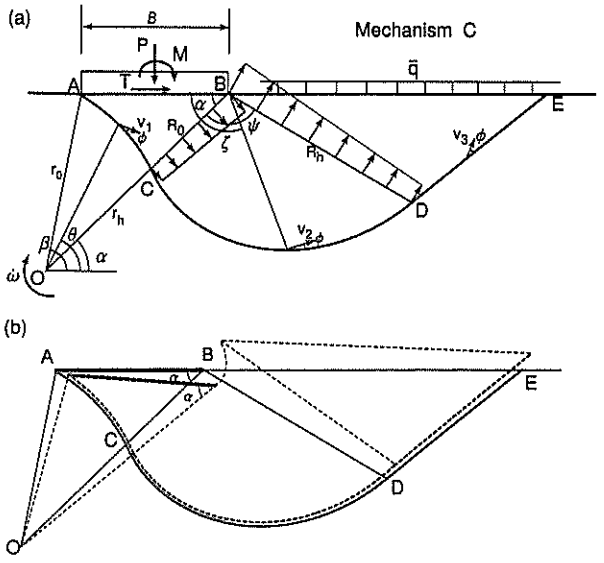

Fig. 5. Rotational collapse mode (Mechanism C): (a) collapse patter; and (b) displacement increments

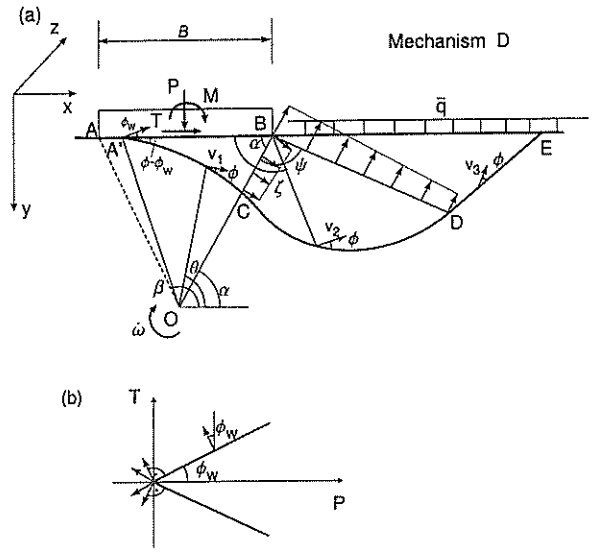

Fig. 6. Rotational mechanism with separation along the footing/soil interface (Mechanism *D*): (a) collapse pattern; and (b) yield condition on the footing/soil interface

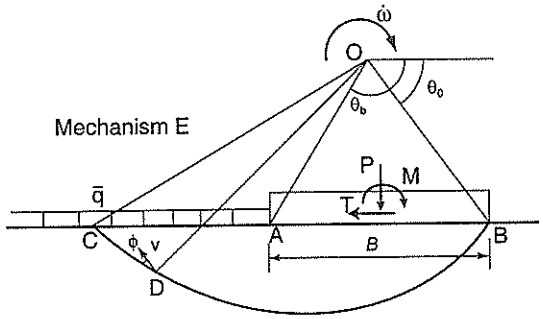

Fig. 7. Rigid rotation collapse (Mechanism *E*)

(1995), both for purely cohesive soils. The last mechanism, Fig. 7, is associated with a simple rigid-rotation mode.

The mechanisms of failure will be described briefly. The first two collapse patterns, *A* and *B*, and the method for calculations of the bearing capacity were discussed in a recent paper (Michalowski, 1997). The foundation soil is divided into rigid blocks, Figs. 2(a) and 3(a), separated by failure surfaces (velocity discontinuities). The velocity boundary condition is velocity V_0 of the footing. Velocities of all blocks and the velocity discontinuity vectors can be calculated as functions of V_0 from the geometrical relations in the hodographs, Figs. 2(b), (c), 3(b). The work dissipation rate is calculated on all discontinuity surfaces (it is zero if the soil is cohesionless). The rate of work dissipation is then equated to the sum of the work-rate of the unknown vertical limit load (unknown bearing capacity), the rate of the work due to the horizontal load (given as part of the vertical load, $\tan\delta$), the work-rate of surcharge load $\bar{q}$, and the rate of work of the soil weight (*see* inequality in (4)). An upper bound estimate of the vertical bearing capacity is obtained from such an equation. The geometry of the mechanism needs to be optimized such that the obtained limit load is minimum (best upper bound).

For a case of weightless soil ($\gamma=0$), a closed-form solution was found for the upper bound on the horizontal limit load causing translation of the footing in the horizontal direction. This failure mechanism is shown in Fig. 4(a), with the hodograph in Fig. 4(b). Since the footing moves horizontally, the solution is not sensitive to the vertical loading (the rate of work of the vertical load is zero). The maximum average limit horizontal load p_t is

$$p_t=c(1+\sin\varphi)e^{((\pi/2)+\varphi)\tan\varphi}+\bar{q}\tan\varphi\,(1+\sin\varphi)e^{((\pi/2)+\varphi)\tan\varphi} \tag{5}$$

or

$$p_t=cN_c'+\bar{q}N_q' \tag{6}$$

where $\bar{q}$ is the surcharge load, and

$$N_c'=(1+\sin\varphi)e^{((\pi/2)+\varphi)\tan\varphi},\quad N_q'=N_c'\tan\varphi. \tag{7}$$

The expressions for the rate of energy dissipation and the rate of work of external load are given in Appendix A.

The mechanism in Fig. 5(a) is described here in more detail. The footing and region ABC rotate as one rigid body about point *O*. Line AC is a log-spiral

$$r=r_0e^{(\theta-\beta)\tan\varphi} \tag{8}$$

where φ is the internal friction angle (*see* Fig. 5(a) for other symbols). The magnitude of the velocity discontinuity vector along AC is

$$v_1=\dot{\omega}r_0e^{(\theta-\beta)\tan\varphi} \tag{9}$$

where $\dot{\omega}$ is the rate of rotation about point *O*. Note that $\theta-\beta<0$, and both *r* and *v* are descending from *A* to *C*. Kinematical admissibility requires that all velocity discontinuity vectors be inclined to the discontinuity surfaces at angle of internal friction φ. Line CD is a segment of another log-spiral, and DE is a straight line segment. The entire line ACDE is a velocity discontinuity (failure surface). The soil in region BCD is subjected to shear deformation. Velocities along CB are all perpendicular to CB, and increase toward *B*, consistently with the rotation about *O*. The magnitude of the velocity discontinuity vector along CD increases according to an exponential law

$$v_2=v_Ce^{(\zeta-\alpha)\tan\varphi} \tag{10}$$

where $v_C=\dot{\omega}\overline{OC}$ is the velocity at point *C*, and ζ is measured from the horizontal, as shown in Fig. 5(a). The velocities at singular point *B* change according to the same law, except the initial velocity is $v_B=\dot{\omega}\overline{OB}$. The velocities are distributed according to a linear function on all radii between point *B* and any point on line CD. The soil in region BDE is subjected to a combination of simple shear and rigid translation. The velocity discontinuity vector along line DE is constant. Incremental displacements are shown in Fig. 5(b) to better illustrate the mechanism.

In summary, line ACDE is a trace of the velocity discontinuity surface, region ABC rotates in a rigid manner, area BCD is subjected to shear, and BDE undergoes a

combination of rigid translation and simple shear. Line ACDE is smooth, and lines BC and BD are not velocity discontinuities.

Based on this mechanism, the work dissipation rate associated with incipient failure was calculated and equated to the work rate of external forces (soil weight, surcharge load $\bar{q}$, and the footing load P, T, and M). This equation yields an upper bound to the bearing capacity P (while T and M are given directly, or in terms of force inclination, $\tan\delta = T/P$, and eccentricity, $e = M/P$). Closed-form expressions were found for the respective work terms, and they are given in Appendix B. Three parameters fully determine the geometry of this mechanism. Angles α, β, and ψ were used in calculations as the three independent parameters. These angles were varied in an optimization procedure (with a minimum increment of 0.01°) where the minimum of the bearing capacity was sought, since this approach leads to the upper bound on the true limit load.

The mechanism in Fig. 6(a) is similar to that in Fig. 5(a) with the exception that the center of rotation is now directly underneath the footing. The footing-soil interface is considered a frictional and unilateral constraint, and the footing can separate from the soil (no adhesion). Since the upper bound approach is used, the mechanism must conform to the normality rule for both the soil deformation and interface interaction. Kinematical admissibility requires that the separation vector be inclined to the interface at an angle not less than the angle of interface friction, φ_w (*see* Fig. 6(b)), and the discontinuity vector be inclined at φ to line A′C. Consequently, discontinuity A′C must approach the soil-foundation interface at angle $\varphi - \varphi_w$. Calculations are similar to those in the case of mechanism C, and they are not presented here.

Mechanism E in Fig. 7 involves rigid rotation of the region between ground surface BAC and the log-spiral BDC. This mechanism becomes critical when a clockwise rotation of the footing is caused by a clockwise moment which is accompanied by a leftward horizontal force component. If the horizontal force component acts in the opposite direction, either mechanism C or D become more critical. This mechanism was earlier considered by Narita and Yamaguchi (1989), and the details of the analysis are omitted here.

RESULTS OF NUMERICAL STUDIES

The bearing capacity of nonsymmetrically loaded strip footings was analyzed using the kinematic approach of limit analysis and the mechanisms presented in the previous section. The analysis had two objectives: (1) to test expressions used in practice for load inclination coefficients in the bearing capacity formula, and (2) to assess the commonly used approximation introduced by Meyerhof (1953), which suggests that the moment load can be included in design by reducing the effective footing width by twice-the-eccentricity.

Cross-sections of the failure surface for a nonsymmetrically loaded footing are shown in Fig. 8 on plane $P/\gamma B^2$,

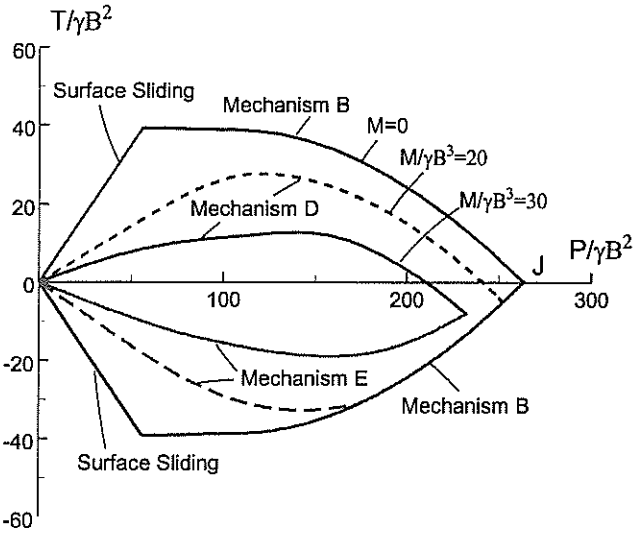

Fig. 8. Failure envelopes for a strip footing ($\varphi = 35°$, $C/\gamma B = 5$, $\bar{q} = 0$)

$T/\gamma B^2$ for different moments $M/\gamma B^3$. The symmetrical mechanism in Fig. 2(a) leads to a bearing capacity independent of moment and load inclination, and it is depicted in Fig. 8 by point J (mechanism A). The nonsymmetrical mechanism B (Fig. 3(a)) yields the best upper estimate of the bearing capacity when the load is inclined with no eccentricity (*see* cross section for $M=0$). The rotational mechanism C (Fig. 5(a)) is also capable of yielding good estimates when $M=0$; in this case the center of rotation (O) tends to reach a large depth, and the mechanism becomes virtually translational. The bearing capacity curve for $M=0$ is symmetric, i.e., the limit load is independent of the sense of the horizontal load. For load inclination angles larger than about 23° the horizontal load component becomes independent of the vertical load, and the footing failure is associated with a horizontal translation similar to that in Fig. 4(a) (although the weight of the soil is accounted for in Fig. 8). This translation is predicted by the flow rule in Eq. (3) associated with the failure criterion in Fig. 8. Adhesion on the footing-soil interface was not considered, thus the surface footing resistance to horizontal loads is limited by the interface friction $T = N\tan\varphi_w$.

Once the moment (or eccentricity) increases, the bearing capacity becomes sensitive to rotation, and, therefore, the rotational mechanisms in Figs. 6 and 7 yield the best upper bounds to the true limit load. Whether mechanism D or E gives better estimates depends on the combination of horizontal load T and moment M. Considering the right-handed coordinate system as in Fig. 6(a), all loads, as shown, are positive. In such case mechanism D gives the best results. If, however, the moment and the horizontal force are of opposite signs, mechanism E (Fig. 7) yields better estimates of bearing capacity. The respective segments of the failure criterion in Fig. 8 are marked as mechanisms B, D or E. Points with tangents parallel to axis $P/\gamma B^2$ can be identified on limit curves for both D or E mechanisms. They imply cases where failure is associated with the footing rotation

about a point directly below the center of the footing. The limit curves associated with two mechanisms are not symmetrical with respect to axis $P/\gamma B^2=0$.

It is also interesting to notice that the interface friction condition, $T=P\tan\varphi_w$, may never be reached if the eccentricity (or moment) is significant, as demonstrated by the curves for $M/\gamma B^3=20$ and $M/\gamma B^3=30$.

The influence of the load inclination and eccentricity is interrelated, as demonstrated in Fig. 8. However, for the purpose of analysis two effects are separated here, so that the existing concept of load inclination factors can be evaluated. Inclination factors, designated usually as i_c, i_q and i_γ, are used as multipliers of the respective terms in the bearing capacity formula

$$p(\delta)=i_c cN_c+i_q qN_q+\frac{1}{2}i_\gamma \gamma BN_\gamma. \tag{11}$$

Coefficients i_c, i_q and i_γ will be derived from three separate analyses. No load eccentricity was considered in analyses of these coefficients. When deriving i_c, both surcharge load $\bar{q}$ and γ were taken as zero; for i_q cohesion c and γ were assumed to be zero; and c and $\bar{q}$ were taken as zero for deriving coefficient i_γ. This allows one to eliminate the influence of cohesion, surcharge load and specific weight on inclination coefficients i_c, i_q and i_γ. The coefficients so calculated are, of course approximate, since, in general, they are not consistent with one mechanism.

For each of the three analyses mentioned in the previous paragraph, the right-hand-side of Eq. (11) is reduced to one term, and, after rearrangement, the following expressions result for the three inclination coefficients

$$i_c=\frac{p(\delta)}{cN_c};\quad q=0,\quad \gamma=0 \tag{12}$$

$$i_q=\frac{p(\delta)}{qN_q};\quad c=0,\quad \gamma=0 \tag{13}$$

$$i_\gamma=\frac{2p(\delta)}{\gamma BN_\gamma};\quad c=0,\quad q=0 \tag{14}$$

where $p(\delta)$ is the vertical component of the bearing pressure calculated using mechanism B in Fig. 3(a). Coefficients N_c and N_q were taken from classical solutions by Prandtl (1920) and Reissner (1924), respectively

$$N_c=(N_q-1)\cot\varphi,\quad N_q=\tan^2\left(\frac{\pi}{4}+\frac{\varphi}{2}\right)e^{\pi\tan\varphi} \tag{15}$$

and coefficient N_γ was derived based on limit analysis of mechanism A in Fig. 2 (Michalowski, 1997)

$$N_\gamma=e^{0.66+5.11\tan\varphi}\tan\varphi. \tag{16}$$

The inclination coefficients so derived then become functions of internal friction angle φ and force inclination angle δ alone, and they are reasonable approximations of the actual influence of the force inclination on the bearing capacity.

The numerical results are given in Fig. 9, for selected values of φ. Closed-form approximate expressions for these coefficients were suggested by Meyerhof (1963),

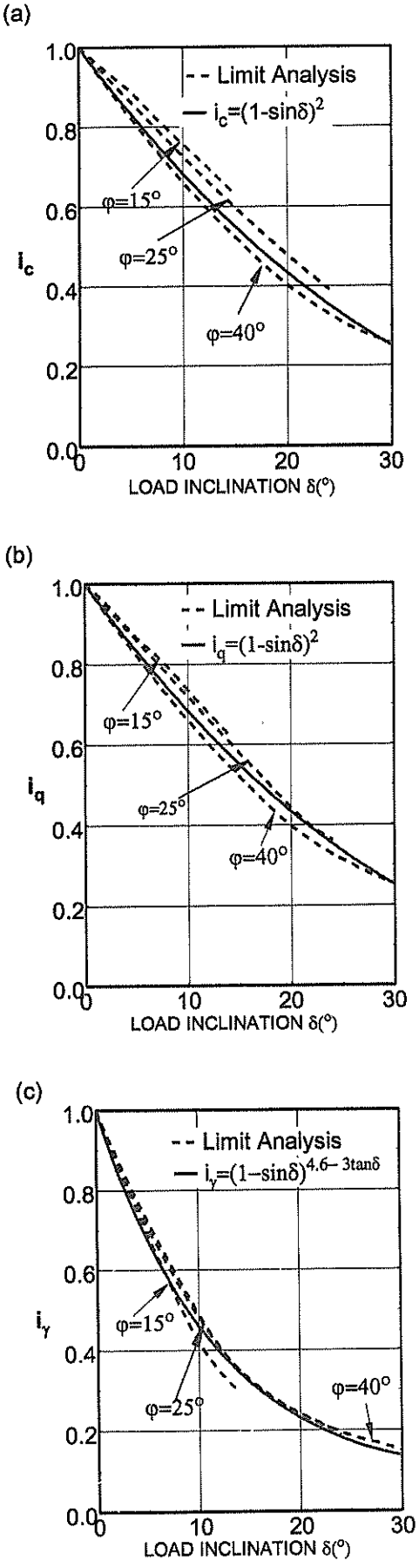

Fig. 9. Calculated coefficients i_c, i_q and i_γ, and the closed-form approximation (solid lines)

Hansen (1970), and Vesic (1975). It was found that the following expressions yield a better fit into the numerical results from limit analysis

$$i_c=i_q=(1-\sin\delta)^2$$
$$i_\gamma=(1-\sin\delta)^{4.6-3\tan\delta} \tag{17}$$

where δ is the inclination angle of the load to the vertical.

The expressions in Eq. (17) seem to match the numerical results from limit analysis well, and it is suggested that they be used for practical purposes.

It was suggested earlier that coefficient i_c be derived based on what is often referred to as a "theorem of correspondence" (Vesic, 1975), which is no more than a transformation rule. This transformation rule is attributed to A. Caquot (*see* De Beer and Ladanyi, 1961). From a plot of the Mohr-Coulomb criterion one can show that the normal stress for a purely frictional soil corresponds to the normal stresses for cohesive-frictional soil (with the same internal friction angle φ) increased by $c\cot\varphi$ (c being the cohesion). This is, for instance, how coefficient N_c in Eq. (15) can be derived once coefficient N_q is known (although, historically, N_c was derived by Prandtl (1920) before N_q was found by Reissner (1924)). This transformation rule, however, is not applicable for inclined traction. If used, coefficient i_c for the cohesive-frictional soil will correspond to an inclination angle different than that for purely frictional soil. The rule can be used, however, when the inclination is zero, since in such case the direction of the traction for both cases coincide. Notice then that this rule of transformation does not apply to the coefficients in Eq. (7).

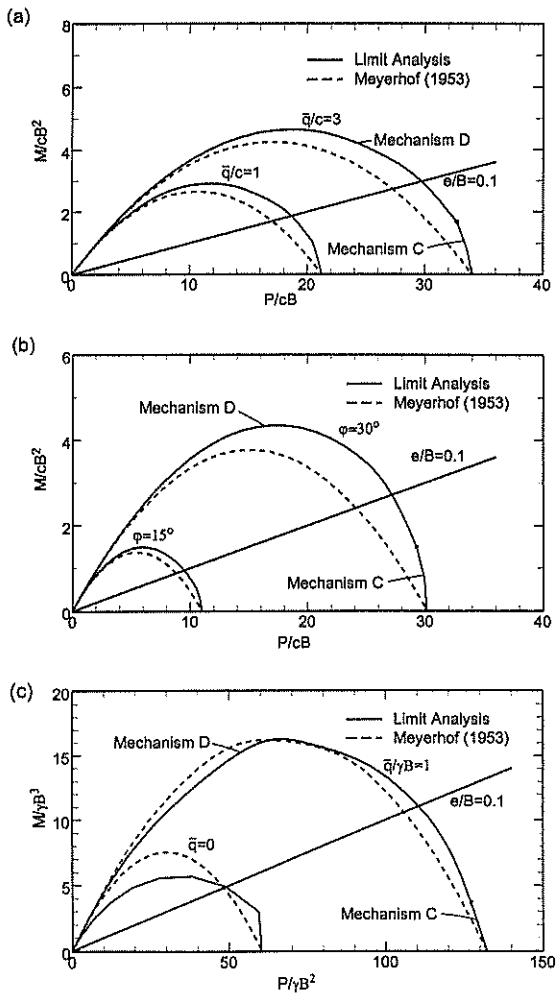

Fig. 10. The influence of moment on bearing capacity: (a) $\gamma=0$, $\varphi=20°$; (b) $\gamma=0$, $\bar{q}=0$; and (c) $c=0$, $\varphi=40°$.

The numerical results from calculations of bearing capacity of footings subjected to eccentric loads (moments) are presented in Fig. 10. The axes of the coordinate system represent dimensionless moment M and limit vertical force P on the footing (both M and P are per unit length of the footing). A straight line drawn from the coordinate origin depicts points of constant relative eccentricity; lines for $e/B=0.1$ are marked on Figs. 10(a)–(c). All examples are given for $\delta=0$ and different combinations of surcharge load. The limit analysis results are compared to those suggested by Meyerhof (1953) where the calculations are performed for a symmetrically loaded footing, but with the width reduced by $2e$ (e-eccentricity).

Mechanism D appeared to be most critical for the range of parameters calculated, except for cases where eccentricity was very small (mechanism C yields a better upper bound estimate for small e/B; *see* Fig. 10).

It can be concluded from the numerical results that the suggestion of Meyerhof, for soils with cohesion, is somewhat conservative when compared to limit analysis (Fig. 10(a), (b)). This conclusion does not come as a surprise, and it can be supported by a more analytical argument. The general expression for the bearing capacity based on mechanism C is given in Eq. (36). A similar expression for mechanism D (and $\delta=0$) can be derived as

$$\frac{P}{cB}=\frac{\sum_1^5 g_i'-\frac{\bar{q}}{c}g_6'}{\frac{e}{B}+\frac{1}{2}+\frac{r_0}{B}\cos\beta}\left(\frac{r_0}{B}\frac{\sin\beta}{\sin\alpha}\right)^2$$
$$=\frac{\sum_1^5 g_i'-\frac{\bar{q}}{c}g_6'}{\frac{e}{B}-\frac{1}{2}+t\cos\alpha}t^2 \tag{18}$$

where r_0/B is given in (28), and t is introduced here for the convenience of differentiating

$$t=\frac{\sin\beta}{\sin(\beta-\alpha)} \tag{19}$$

and coefficients g' are similar to those in Eq. (36) (but divided by t^2). The geometry of the mechanism depends on three variables (angles): α, β and ψ. The best upper bound to bearing capacity can be found when partial derivatives of P/cB with respect to the variables are zero. In Eq. (18) angle β is present only in the expression for t, hence the minimum conditions with respect to β can be written as

$$\frac{\partial}{\partial t}\left(\frac{P}{cB}\right)=0 \tag{20}$$

which leads to

$$t\cos\alpha=1-2\frac{e}{B}. \tag{21}$$

Substituting Eq. (21) into Eq. (18) yields

$$\frac{P}{cB}=2\frac{\sum_1^5 g_i'-\frac{q}{c}g_6'}{\cos^2\alpha}\left(1-2\frac{e}{B}\right). \tag{22}$$

The multiplier in the parentheses in Eq. (22) is equivalent to Meyerhof's "effective width" hypothesis. However, Meyerhof (1953) suggested that this multiplier be applied to the bearing capacity for centrally loaded footing (not subjected to rotation). A symmetrical mechanism for a footing of width B, but with a wedge of width $B-2e$, is kinematically inadmissible, and an estimate of bearing capacity should be expected to be conservative (as shown in Fig. 10(a), (b)). Nevertheless, Meyerhof's suggestion seems to be reasonable for soils with cohesion. However, the same argument cannot be used for purely frictional soils, where the Meyerhof's hypothesis may lead to an overestimate of the bearing capacity (Fig. 10(c)).

FINAL REMARKS

The kinematic approach of limit analysis was applied to the problem of bearing capacity of surface strip footings subjected to nonsymmetrical loads. This approach leads to a strict upper bound to limit loads. If the bearing capacity is to be sensitive to the load inclination or its eccentricity, the mechanism used in the analysis must be nonsymmetrical. Otherwise, the work rate of the nonsymmetrical part of the load is equal to zero, and the calculated vertical limit load (bearing capacity) becomes independent of the magnitude of both the horizontal component of the force and the moment.

Closed-form expressions are suggested for inclination coefficients to be used in the bearing capacity formula. These coefficients are derived as an analytical approximation to numerical results, and they fit these results better than those suggested earlier in the literature. It is also noted in the paper that the transformation rule (often called the "theorem of correspondence") is not applicable for deriving the inclination coefficient associated with cohesion, as suggested in some earlier papers on the subject.

The same approach was used to assess the influence of the eccentricity on the bearing capacity. An often-used method (suggested by Meyerhof, 1953) where the footing width is reduced by twice-the-eccentricity was found to be conservative for soils with cohesion. This is consistent with findings of Salençon and Pecker (1995). However, for purely frictional soils, this method can lead to an overestimation of the true bearing capacity. Whereas Meyerhof's technique leads to an inadmissible failure mechanism when interpreted in terms of limit analysis, it has been widely accepted because of its simplicity.

ACKNOWLEDGEMENT

The work presented in this paper was supported by the National Science Foundation, grant No. CMS-9634193. This support is greatly appreciated.

REFERENCES

1) Gottardi, G. and Butterfield, R. (1993): "On the bearing capacity of surface footings on sand under general planar loads," Soils and Foundations, Vol. 33, No. 3, pp. 68–79.
2) De Beer, E. E. and Ladanyi, B. (1961): "Etude expérimentale de la capacité portante du sable sous des fondations circulaires établies en surface," Proc. 5th Int. Conf. on SMFE, Paris, Vol. 1, pp. 577–581.
3) Hansen, J. B. (1970): "A revised and extended formula for bearing capacity," Geoteknisk Inst., Bulletin, Vol. 28, pp. 5–11.
4) Koiter, W. T. (1953): "Stress-strain relations, uniqueness and variational theorems for elastic-plastic materials with a singular yield surface," Quart. Appl. Math., Vol. 11, pp. 350–354.
5) Meyerhof, G. G. (1953): "The bearing capacity of foundations under eccentric and inclined loads," 3rd Int. Conf. on SMFE, Zürich, Vol. 1, pp. 440–445.
6) Meyerhof, G. G. (1963): "Some recent research on the bearing capacity of foundations," Can. Geotech. J., Vol. 1, No. 1, pp. 16–26.
7) Michalowski, R. L. (1997): "An estimate of the influence of soil weight on bearing capacity using limit analysis," Soils and Foundations, Vol. 37, No. 4, pp. 57–64.
8) Murff, J. D. and Miller, T. W. (1977): "Foundation stability on nonhomogeneous clays," J. Geotech. Engrg. Div., Vol. 103, No. 10, pp. 1083–1096.
9) Narita, K. and Yamaguchi, H. (1989): "Analysis of bearing capacity for log-spiral sliding surfaces," Soils and Foundations, Vol. 29, No. 2, pp. 85–98.
10) Prager, W. (1955): "The general theory of limit design," Proc. 8th Int. Congress Theoretical and Applied Mechanics, Istambul 1952, pp. 65–72.
11) Prandtl, L. (1920): "Über die Härte plastischer Körper," Nachr. Ges. Wissensch, Göttingen, math.-phys. Klasse, 1920, pp. 74–85.
12) Reissner, H. (1924): "Zum Erddruckproblem," in Proc., 1st Int. Congress for Applied Mechanics, Biezeno, C. B. and Burgers, J. M. (eds.), Delft, pp. 295–311.
13) Salençon, J. and Pecker, A. (1995): "Ultimate bearing capacity of shallow foundations under inclined and eccentric loads. Part I: purely cohesive soil," Eur. J. Mech. A/Solids, Vol. 14, No. 3, pp. 349–375.
14) Vesic, A. S. (1975): "Bearing capacity of shallow foundations," in: Foundation Engineering Handbook, Winterkorn, H. F. and Fang, H. Y. (eds.), Van Nostrand, pp. 121–147.

APPENDIX A

The expression for the limit horizontal load was obtained using the upper bound theorem with the work terms derived from the geometric relations in Fig. 4. The rate of energy dissipation along discontinuity AC is

$$\dot{D}_{AB}=BcV_0 \tag{23}$$

where B is the width of the footing, c is the cohesion, and V_0 is the horizontal velocity of the footing. The dissipation rates along the log-spiral discontinuity DE, and the combined rate along CD and within BCD are

$$\dot{D}_{DE}=BcV_0\sin\varphi\, e^{((\pi/2)+\varphi)\tan\varphi} \tag{24}$$

and

$$\dot{D}_{BCD}=BcV_0[e^{((\pi/2)+\varphi)\tan\varphi}-1] \tag{25}$$

respectively. The footing undergoes horizontal translation only, thus the work rate of the footing load is independent of the vertical load and moment

$$\dot{W}_p=p_tBV_0 \tag{26}$$

and the rate of work of the surcharge load is

$$\dot{W}_q=-B\bar{q}V_0\tan\varphi\,(1+\sin\varphi)e^{((\pi/2)+\varphi)\tan\varphi}. \tag{27}$$

Equating the rate of work of the external force (Eqs. (26), (27)) to the rate of work dissipation (Eqs. (23)–(25)) one obtains the expression for the upper bound to the horizontal load in Eq. (5).

APPENDIX B

The following relations can be derived from the geometry in Fig. 5(a):

$$\begin{aligned}&\frac{r_0}{B}=\frac{\sin\alpha}{\sin(\beta-\alpha)}, && \frac{r_h}{B}=\frac{r_0}{B}e^{(\alpha-\beta)\tan\varphi}\\ &\frac{R_0}{B}=\frac{\sin\beta}{\sin(\beta-\alpha)}-\frac{r_h}{B}, && \frac{R_h}{B}=\frac{R_0}{B}e^{\psi\tan\varphi}\end{aligned} \tag{28}$$

The rate of external loads P, T, and M can be written as

$$\dot{W}=PB\dot{\omega}\left[\frac{1}{2}+\frac{r_0}{B}(\cos\beta+\sin\beta\tan\delta)+\frac{e}{B}\right] \tag{29}$$

where $\dot{\omega}$ is the rate of rotation about point O (Fig. 5(a)), and $\delta=T/P$ and $e=M/P$. The energy dissipation rate along segment AC of the velocity discontinuity is

$$\dot{D}_{AC}=cB^2\dot{\omega}\left(\frac{r_h}{B}\right)^2\frac{1}{2\tan\varphi}[e^{2(\beta-\alpha)\tan\varphi}-1]=cB^2\omega g_1 \tag{30}$$

where c is the soil cohesion. The rates of energy dissipation along discontinuity segments CD and DE are

$$\dot{D}_{CD}=cB^2\dot{\omega}\frac{R_0r_h}{2B^2\tan\varphi}[e^{2\psi\tan\varphi}-1]=cB^2\dot{\omega}g_2 \tag{31}$$

and

$$\dot{D}_{DE}=cB^2\dot{\omega}\frac{R_hr_h}{2B^2}\frac{\cos\varphi\sin(\alpha+\psi)}{-\cos(\alpha+\psi-\varphi)}e^{\psi\tan\varphi}-cB^2\dot{\omega}g_3 \tag{32}$$

respectively. The rates of dissipation in regions BCD and BDE are

$$\dot{D}_{BCD}=cB^2\dot{\omega}\frac{R_0(R_0+r_h)}{2B^2\tan\varphi}[e^{2\psi\tan\varphi}-1]=cB^2\dot{\omega}g_4 \tag{33}$$

and

$$\dot{D}_{BDE}=cB^2\dot{\omega}\frac{R_0R_h}{2B^2}\frac{\cos\varphi\sin(\alpha+\psi)}{-\cos(\alpha+\psi-\varphi)}e^{\psi\tan\varphi}=cB^2\dot{\omega}g_5 \tag{34}$$

respectively. The rate of work of the surcharge load along BE, during incipient flow, is

$$\begin{aligned}\dot{W}_q&=qB^2\dot{\omega}\left[\frac{\cos\varphi\cos(\alpha+\psi)}{-2\cos(\alpha+\psi-\varphi)}\frac{R_h}{B}\left(\frac{R_0}{B}+2\frac{r_h}{B}\right)e^{\psi\tan\varphi}\right]\\&=\bar{q}B^2\dot{\omega}g_6\end{aligned} \tag{35}$$

where $\bar{q}$ is the magnitude of the surcharge load. The upper bound to the bearing capacity of the strip footing subjected to the rotational mechanism in Fig. 5(a) was derived as

$$\frac{P}{cB}=\frac{\sum_1^5 g_i-\dfrac{\bar{q}}{c}g_6}{\dfrac{1}{2}+\dfrac{e}{B}+\dfrac{r_0}{B}(\cos\beta+\sin\beta\tan\delta)} \tag{36}$$

where coefficients g_i are given in Eqs. (30)–(35).